JCI The Journal of Clinical Investigation

Mature T cell responses are controlled by microRNA-142

Yaping Sun, … , Thomas Saunders, Pavan Reddy

J Clin Invest. 2015;125(7):2825-2840. https://doi.org/10.1172/JCI78753.

Research Article **Immunology**

T cell proliferation is critical for immune responses; however, the molecular mechanisms that mediate the proliferative response are poorly understood. MicroRNAs (miRs) regulate various molecular processes, including development and function of the immune system. Here, utilizing multiple complementary genetic and molecular approaches, we investigated the contribution of a hematopoietic-specific miR, miR-142, in regulating T cell responses. T cell development was not affected in animals with a targeted deletion of *Mir142*; however, T cell proliferation was markedly reduced following stimulation both in vitro and in multiple murine models of graft-versus-host disease (GVHD). miR-142–deficient T cells demonstrated substantial cell-cycling defects, and microarray and bioinformatics analyses revealed upregulation of genes involved in cell cycling. Moreover, 2 predicted miR-142 target genes, the atypical E2F transcription factors *E2f7* and *E2f8*, were most highly upregulated in miR-142–deficient cells. Clustered regularly interspaced short palindromic repeat interference–mediated (CRISPRi-mediated) silencing of E2F7 and E2F8 in miR-142–deficient T cells ameliorated cell-cycling defects and reduced GVHD, and overexpression of these factors in WT T cells inhibited the proliferative response. Together, these results identify a link between hematopoietic-specific miR-142 and atypical E2F transcription factors in the regulation of mature T cell cycling and suggest that targeting this interaction may be relevant for mitigating GVHD.

Mature T cell responses are controlled by microRNA-142

Yaping Sun,[1] Katherine Oravecz-Wilson,[1] Nathan Mathewson,[1,2] Ying Wang,[1] Richard McEachin,[3] Chen Liu,[4] Tomomi Toubai,[1] Julia Wu,[1,2] Corinne Rossi,[1] Thomas Braun,[5] Thomas Saunders,[6] and Pavan Reddy[1]

[1]Department of Internal Medicine, Division of Hematology/Oncology, University of Michigan Comprehensive Cancer Center, Ann Arbor, Michigan, USA. [2]Graduate Program in Immunology and [3]Center for Computational Medicine and Bioinformatics, University of Michigan Medical School, Ann Arbor, Michigan, USA. [4]Department of Pathology, Immunology and Laboratory Medicine, University of Florida College of Medicine, Gainesville, Florida, USA. [5]Department of Biostatistics and [6]Transgenic Animal Model Core, University of Michigan, Ann Arbor, Michigan, USA.

T cell proliferation is critical for immune responses; however, the molecular mechanisms that mediate the proliferative response are poorly understood. MicroRNAs (miRs) regulate various molecular processes, including development and function of the immune system. Here, utilizing multiple complementary genetic and molecular approaches, we investigated the contribution of a hematopoietic-specific miR, miR-142, in regulating T cell responses. T cell development was not affected in animals with a targeted deletion of *Mir142*; however, T cell proliferation was markedly reduced following stimulation both in vitro and in multiple murine models of graft-versus-host disease (GVHD). miR-142–deficient T cells demonstrated substantial cell-cycling defects, and microarray and bioinformatics analyses revealed upregulation of genes involved in cell cycling. Moreover, 2 predicted miR-142 target genes, the atypical E2F transcription factors *E2f7* and *E2f8*, were most highly upregulated in miR-142–deficient cells. Clustered regularly interspaced short palindromic repeat interference–mediated (CRISPRi-mediated) silencing of E2F7 and E2F8 in miR-142–deficient T cells ameliorated cell-cycling defects and reduced GVHD, and overexpression of these factors in WT T cells inhibited the proliferative response. Together, these results identify a link between hematopoietic-specific miR-142 and atypical E2F transcription factors in the regulation of mature T cell cycling and suggest that targeting this interaction may be relevant for mitigating GVHD.

Introduction

Several lines of evidence have established a critical role for T cells and their proliferation in causing alloantigen- or autoantigen-driven graft-versus-host disease (GVHD), which develops in 30% to 75% of allogeneic hematopoietic stem cell transplant (alloHSCT) recipients and is associated with significant morbidity and mortality (1). The biology of GVHD is complex, but donor T cells are essential for GVHD (1, 2). Although targeted modulation of pathways important for T cell functions has been the traditional approach for reducing GVHD (2), a substantial gap remains in our understanding of the molecular regulation of T cell function for reducing GVHD.

MicroRNAs (miRs, also known as miRNAs) are a family of small, noncoding RNAs. Recent studies have indicated that miRs play critical roles in the development and function of the immune system (3–6). T cell–specific deletion of Dicer revealed a requirement for the miR pathway in the development and function of mature T cells (7, 8). We and other researchers previously reported that miR-142–3p is expressed in hematopoietic cells, such as DCs, monocytes, T cells, and B cells (9, 10). In particular, miR-142 is specifically expressed in hematopoietic cells at homeostasis in a PU-1–dependent manner (9, 11, 12). miR-142 regulates innate immunity by negatively regulating IL-6 expression in DCs (9), and a recent study indicated that miR-142–3p plays critical roles in the maintenance of $CD4^+$ DCs (12). Recent studies have also demonstrated that miR-142–3p prevents macrophage differentiation during tumor-induced myeloid differentiation (13) and megakaryopoiesis (14). But its role in adaptive immunity, specifically for naive T cell development and function, remains unknown. Recently, we showed that miR-142 is among the most dysregulated miRs following allogeneic stimulation of naive T cells (15). Based on these observations, we proposed a model suggesting that miR-142 modulates T cells and critically affects acute GVHD severity and mortality. But the impact of ablation of the *Mir142* gene on T cell function and GVHD development remains unclear.

To characterize the function of miR-142 in T cell immunity, we generated mutant mice with a targeted deletion of the *Mir142* gene on the C57BL/6 (B6) genetic background. The miR-142–deficient mice were viable and fertile and showed normal T cell development, phenotypes, and numbers, demonstrating that miR-142 does not alter normal T cell development and homeostatic proliferation. We performed a series of in vitro and in vivo studies to specifically address whether deficiency of miR-142 in T cells only modulated their function in the presence of miR-142 in other hematopoietic cells. We found that miR-142 deficiency caused reductions in proliferative capacity, apoptosis, and the capacity to secrete IFN-γ and IL-17 following in vitro or in vivo stimulation. These defects resulted in reduction of GVHD in multiple murine models. Targeting miR-142 in vivo with its antagomir further reduced GVHD, thus suggesting that this strategy may represent a novel approach for ameliorating T cell–mediated GVHD. Mechanistic studies showed that miR-142 KO T cells demonstrated defective cell cycling, S and G_2/M phase arrest, and increased expression of cell-cycle–related genes. The alterations in cell cycling were a consequence of increased

Conflict of interest: The authors have declared that no conflict of interest exists.
Submitted: January 14, 2015; **Accepted:** May 14, 2015.
Reference information: *J Clin Invest*. 2015;125(7):2825–2840. doi:10.1172/JCI78753.

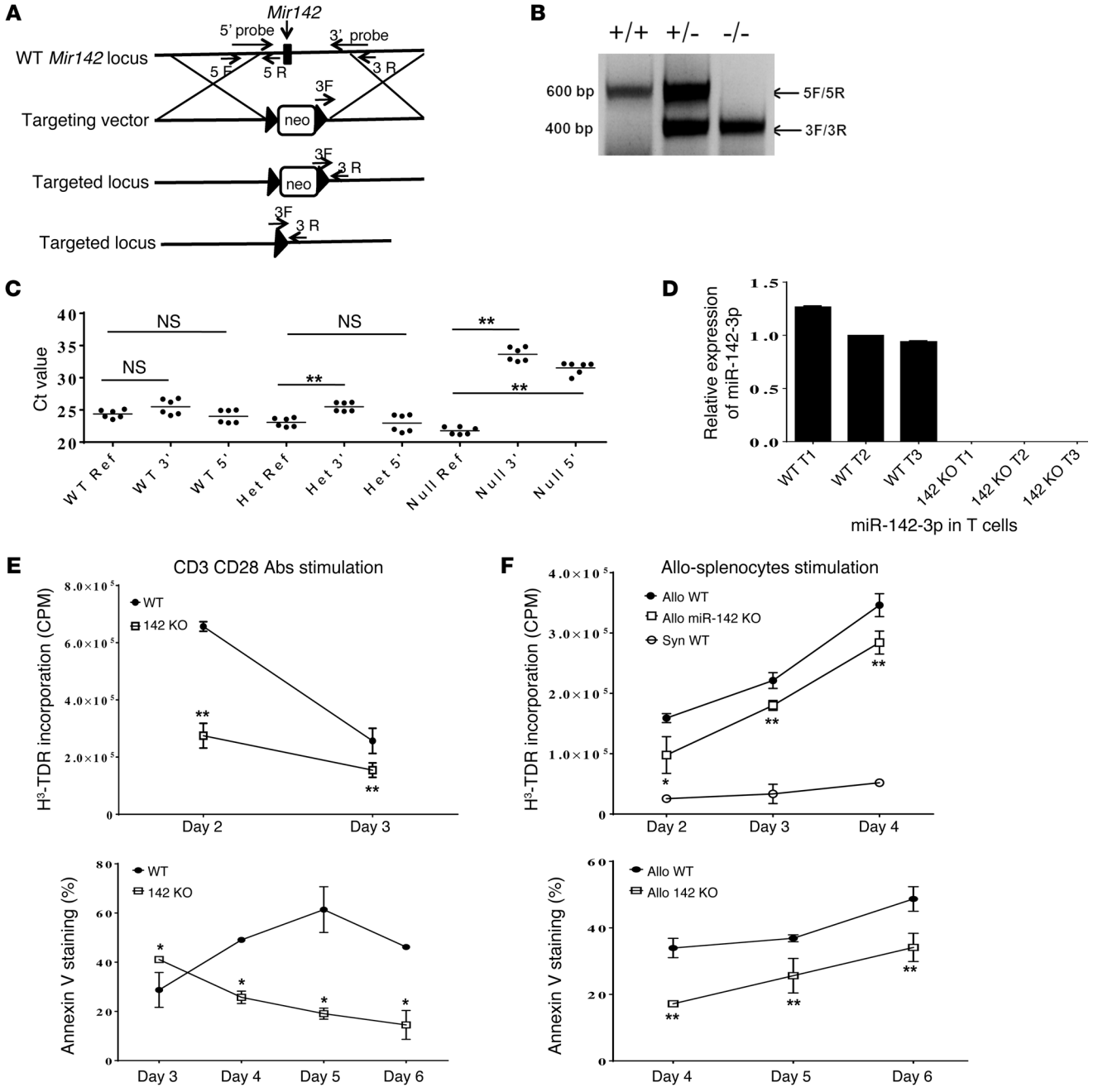

Figure 1. Generation of miR-142 KO mice and its impact on T cell functional responses. (**A**) Scheme of the *Mir142* locus and targeting vector used to generate *Mir142* null alleles. 5′ and 3′ arm probes (5′ probe and 3′ probe) and 5′ and 3′ primers (5F/5R and 3F/3R) for genotyping are shown. (**B**) A representative genotyping result illustrating WT ($Mir142^{+/+}$), heterozygous ($Mir142^{+/-}$), and null mice ($Mir142^{-/-}$). (**C**) Zygosity determination by TaqMan qPCR using Tert as positive control and probes specific for 3′ and 5′ arms designed for *Mir142* gene homologous recombination to confirm the deletion of the *Mir142* gene in homozygous KO mice and single-copy loss in heterozygous mice. Data represent a combination of 6 independent experiments. *P* values were obtained using unpaired *t* test. $^{**}P < 0.01$. (**D**) The loss of miR-142 expression at the RNA level in purified T cells from miR-142 KO mice confirmed by TaqMan qPCR using specific probes against miR-142–3p. Data represent a combination of 3 independent experiments. (**E** and **F**) Significantly reduced proliferation of miR-142 KO T cells determined by tritium incorporation and decreased apoptosis determined by annexin V staining when stimulated in vitro with anti-CD3 and anti-CD28 Abs for 2 to 6 days (**E**) or stimulated in vitro with allogeneic (allo) splenocytes for 2 to 6 days (**F**). Syn, syngeneic. Data shown represent results from 3 or 4 independent experiments (mean ± SEM). *P* values were obtained using the Holm-Sidak method. $^{*}P < 0.05$; $^{**}P < 0.01$.

expression of the atypical E2Fs, E2F7 and E2F8, as confirmed by the overexpression of E2F7 and E2F8 in WT T cells and the targeted silencing of E2F7 and E2F8 in miR-142 KO T cells by the clustered regularly interspaced short palindromic repeat interference (CRISPRi) system in vitro and in vivo. These findings identify miR-142 and its targets E2F7 and E2F8 as molecular regulators of T cell responses and suggest miR-142 inhibition as a potential therapeutic strategy for T cell–mediated GVHD.

Results

Generation of mice with a targeted deletion of the Mir142 gene. The miR-142 locus is located on mouse chromosome 11, and the miR-142 precursor is transcribed from an independent transcriptional unit with its own promoter (11). To experimentally test the biological role of miR-142 in the immune system and to delete the *Mir142* gene and its upstream promoter region, our KO strategy aimed to remove a genomic fragment that included the *Mir142* gene and the 1000-bp upstream region (a transcription promoter region for the *Mir142* gene, ref. 11) to avoid the possible occurrence of B cell lymphoma caused by potential translocations that could occur after germline transmission (refs. 16, 17, and Figure 1A). Tail DNA PCR genotyping confirmed that mice were homozygous KOs for the *Mir142* gene (Figure 1B). Additional zygosity tests were performed using TaqMan quantitative PCR (qPCR) with specific reference probes, as described in Methods. These tests confirmed the deletion of the *Mir142* gene in the genomes of homozygous KO mice and the loss of a single allele in the genomes of heterozygous mice (Figure 1C). The loss of miR-142 expression at the RNA level in BM cells isolated from tibia and fibula was confirmed using TaqMan qPCR with specific probes against miR-142–3p, using Raw264.7 cells as a positive control and NIH3T3 cells as a negative control (ref. 11 and Supplemental Figure 1A; supplemental material available online with this article; doi:10.1172/JCI78753DS1). miR-142–3p was markedly lower in miR-142 KO mice, not only compared with WT and heterozygous mice, but also with positive control Raw264.7 cells and negative control NIH3T3 cells. Importantly, the expression levels of miR-142–3p were relatively high in heterozygous mice (Supplemental Figure 1A), suggesting that miR-142 expression is not impaired in heterozygous mice. Moreover, the absence of miR-142 expression in miR-142 KO mice was further confirmed in purified T cells (Figure 1D and Supplemental Figure 1B) and in other hematopoietic cells such as DCs (data not shown).

Deletion of Mir142 increases expression of its known targets. IL-6 is a known target of *Mir142* in hematopoietic cells (9, 12, 18). Therefore, to confirm whether the deletion of miR-142 had direct effect on its known target IL-6, the splenic DCs were purified from miR-142 KO and WT mice and treated with or without LPS (Supplemental Figure 2). The concentrations of IL-6 and TNF-α in supernatants were measured by ELISA. Significantly higher levels of IL-6, but not TNF-α, were detected in miR-142–deficient DCs compared with DCs isolated from WT mice (Supplemental Figure 2, A and B). Similarly, significantly higher *Il6* mRNA expression was detected by microarray analysis (Supplemental Figure 2C). Expression of adenylyl cyclase 9 (AC9), another miR-142–3p target (19), was elevated in miR-142 KO T cells (Supplemental Figure 2D). These data confirmed the successful establishment of a miR-142 KO mouse model and confirmed IL-6 and AC9 as targets of miR-142–3p, as was previously reported by us (9) and others (19).

Effect of miR-142 deficiency on T cell development. We next determined whether miR-142 deficiency affected T cell development. Analyses of BM cells revealed that there were similar numbers of $Lin^-Sca1^+c\text{-}Kit^+$ hematopoietic stem cells (HSCs) in miR-142 KO mice compared with WT littermates (Supplemental Figure 3A). In addition, there were similar numbers of T cell precursors $Lin^-Sca1^+c\text{-}Kit^+lL\text{-}7Ra^+$ in BM of the miR-142 KO mice and the WT littermates (Supplemental Table 3). Thymic analyses revealed no significant differences in total thymocytes in double-positive, double-negative, or single-positive $CD4^+$ or $CD8^+$ thymocytes between WT and KO animals (Supplemental Figure 3B). Analyses of secondary lymphoid organs revealed no differences in the numbers of total, naive, central memory, and effector memory T cells between the WT and KO animals (Supplemental Figure 3C). These data suggest that miR-142 deficiency did not lead to impaired thymopoiesis or T cell differentiation at homeostasis in naive animals under specific pathogen–free (SPF) conditions.

Deficiency of miR-142 in T cells alters in vitro responses. We determined the impact of miR-142 deficiency on T cell functions in a cell-autonomous manner. To this end, purified T cells were stimulated in vitro with anti-CD3 and anti-CD28 Abs for 2 to 6 days. Compared with WT T cells, miR-142 KO T cells showed significantly reduced proliferation, as determined by ^{3}H-TdR incorporation, but they underwent less apoptosis after day 4 (Figure 1E). Similar results were observed upon stimulation with allogeneic splenocytes (Figure 1F). ELISA measurements showed that the reduction in T cell proliferation was associated with less production of IFN-γ, IL-17A, and IL-2, but more production of IL-6 upon stimulation with anti-CD3 and anti-CD28 Abs or allogeneic splenocytes, consistent with our previous observations from knockdown (KD) studies (ref. 9 and Figure 2, A–C). We further confirmed the expression profile of cytokines in miR-142–deficient T cells after anti-CD3 and anti-CD28 Ab stimulation with intracellular cytokine staining and observed significantly decreased percentages and absolute numbers of miR-142–deficient T cells that stained positively for IFN-γ, IL-17A, and IL-2 compared with WT T cells (Figure 2D). The reduced expansion of T cells may have also contributed to the overall reduction in cytokine levels.

miR-142 KO T cells show altered T cell proliferative responses in vivo. To determine whether miR-142 deficiency in T cells affects their in vivo functions in a cell-autonomous manner, without the confounding effects from the absence of miR-142 in other hematopoietic cells, we examined the effects of miR-142 deficiency on T cell responses following in vivo allogeneic stimulation. We also chose this model because previous study demonstrated significant alterations in the expression of miR-142 in T cells following allostimulation (15). We utilized a well-characterized T cell–dependent MHC disparate allogeneic bone marrow transplant (BMT) model (B6 into BALB/c) and performed BMT with 1×10^6 cells from WT-Ly5.2/CD45.1, or *Mir142*$^{-/-}$-Ly5.1/CD45.2 along with WT T cell–depleted (TCD) BM (5×10^6) into BALB/c. Consistent with in vitro studies, the allogeneic miR-142–deficient donor T cells showed significantly reduced expansion in recipient spleens and mesenteric lymph nodes (mLNs) on day 7 after BMT when compared with allogeneic animals that received WT T cells (Figure 3, A and B). Additional experiments that followed a design similar to that shown in Figure 3A and Figure 2B, but with the administration of BrdU (50 mg/kg in 0.9% saline) to mice 3 hours prior to tissue collection, showed reduced BrdU incorporation in the allogeneic miR-142 KO T cells compared with WT T cells (Figure 3, C and D). The reduced in vivo expansion of miR-142 KO T cells was associated with reduced production of IFN-γ and IL-17A (Figure 3E). Analyses of transferred donor T cells demonstrated reduced recovery of both donor $CD4^+$ and $CD8^+$ T cell populations and reduced activated T cells ($CD4^+CD25^+$, $CD4^+CD62L^-$, and $CD8^+CD62L^-$)

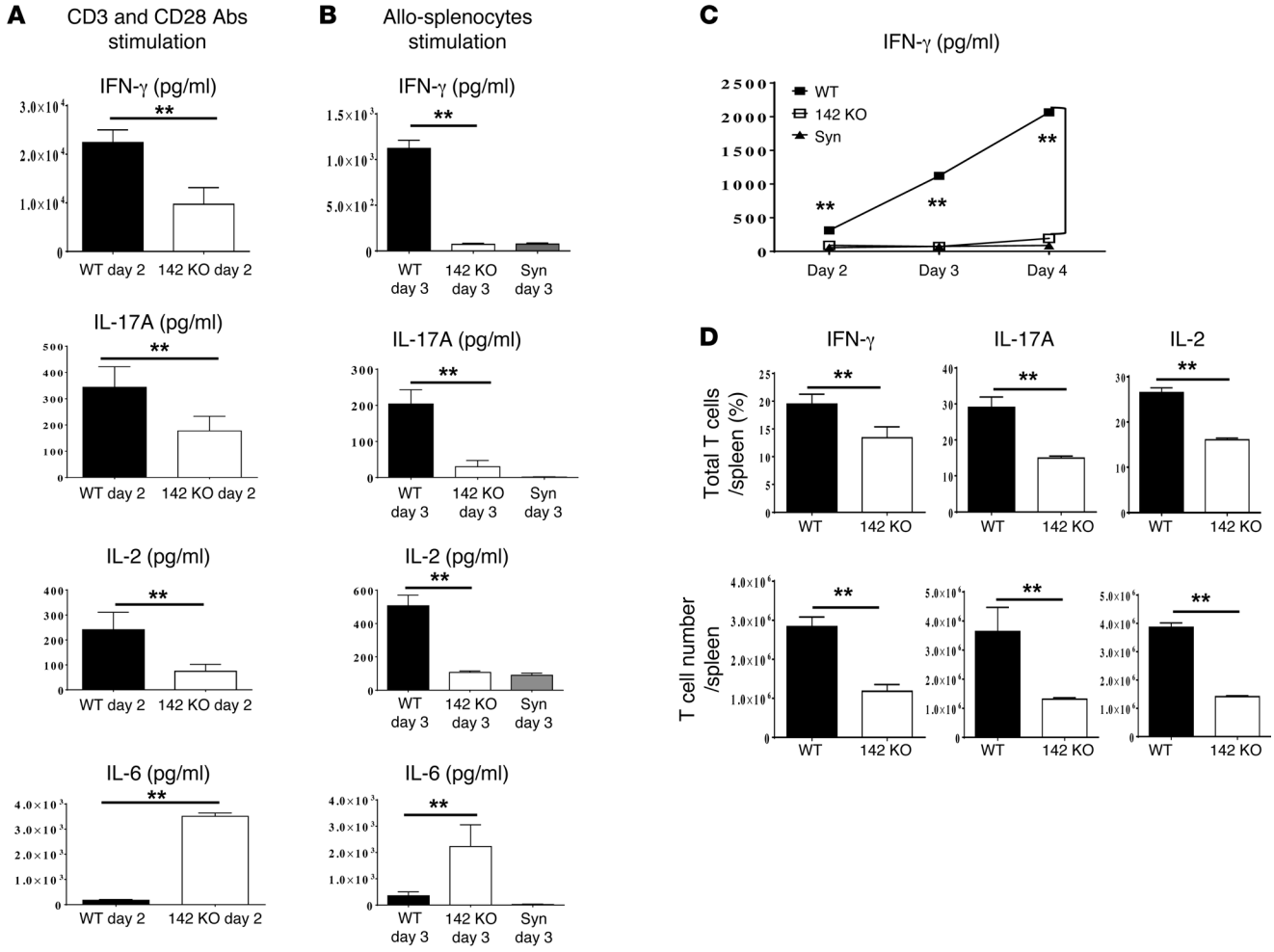

Figure 2. miR-142 KO T cells altered in cytokine expression and proliferative responses in vitro. (**A** and **B**) ELISA measurements demonstrated significantly lower production of IFN-γ, IL-17A, and IL-2, but greater IL-6 production in miR-142 KO T cells compared with WT T cells when stimulated with anti-CD3 and anti-CD28 Abs (**A**) or allogeneic splenocytes (**B**). Combined results were from 3 independent experiments (mean ± SEM). *P* values were obtained using unpaired *t* test. (**C**) Less IFN-γ production was dynamically observed from 2 to 4 days in miR-142 KO T cells compared with WT T cells when stimulated with anti-CD3 and anti-CD28 Abs. Combined results were from 3 independent experiments (mean ± SEM). *P* values were obtained using the Holm-Sidak method. (**D**) Lower percentages and absolute numbers of T cells expressing IFN-γ, IL-17A, and IL-2 in miR-142 KO T cells compared with WT mice. Splenic T cells isolated from WT or miR-142 KO mice were treated with 1× cell stimulation cocktail (plus protein transport inhibitors 1:500, eBioscience, 00-4975) for 6 hours, stained for APC-conjugated CD90.2, then processed for fixation and permeabilization and incubated in a predetermined optimum concentration of PE-conjugated Abs of interest (against IFN-γ, IL-17A, or Il-2). Positive-stained T cells for IFN-γ, IL-17A, and IL-2 were analyzed as described in Methods. Combined results were from 3 independent experiments (mean ± SEM). *P* values were obtained using unpaired *t* test. $^{**}P < 0.01$.

and memory T cells ($CD4^+CD44^+$ and $CD8^+CD44^+$). Furthermore, the numbers of exhausted donor T cells ($CD4^+PD\text{-}1^+$, $CD4^+LAG^+$, $CD8^+PD\text{-}1^+$ and $CD8^+LAG3^+$) were also reduced in the allogeneic recipients that received naive miR-142 KO T cells when compared with WT T cell recipients (Figure 3F).

To further examine whether the reduced in vivo proliferation was a consequence of a T cell–intrinsic deficiency, we cotransferred Ly5.2 WT and Ly5.1 miR-142–deficient T cells into irradiated allogeneic BALB/c recipient mice. Donor miR-142 KO T cells showed significantly reduced expansion in the spleen and mLNs compared with WT donor T cells, as shown by absolute numbers and ratios (Figure 3, G and H), demonstrating that the reduced proliferation and expansion of miR-142–deficient T cells are attributable to cell-autonomous features rather than extrinsic environmental factors. Together, these data demonstrate that the reduced proliferation capacity of miR-142–deficient T cells was a consequence of cell-intrinsic features rather than environmental influences.

miR-142 KO T cells induce less severe GVHD in multiple models of allogeneic BMT. We next assessed whether the reduced in vivo proliferation of miR-142 KO T cells has biological relevance by determining the effect on GVHD severity utilizing 3 distinct models. First, in the MHC and minor histocompatibility antigens disparate B6 ($H2^b$) into BALB/c ($H2^d$) model, the congenic B6 animals served as the syngeneic controls. BALB/c recipient mice were lethally irradiated (800 cGy total body irradiation [TBI], split dose) and transplanted and monitored for GVHD as described in Methods. All of the syngeneic animals survived, but the allogeneic animals that received WT T cells died with signs of severe GVHD. In contrast, the allogeneic animals that received miR-142 KO T

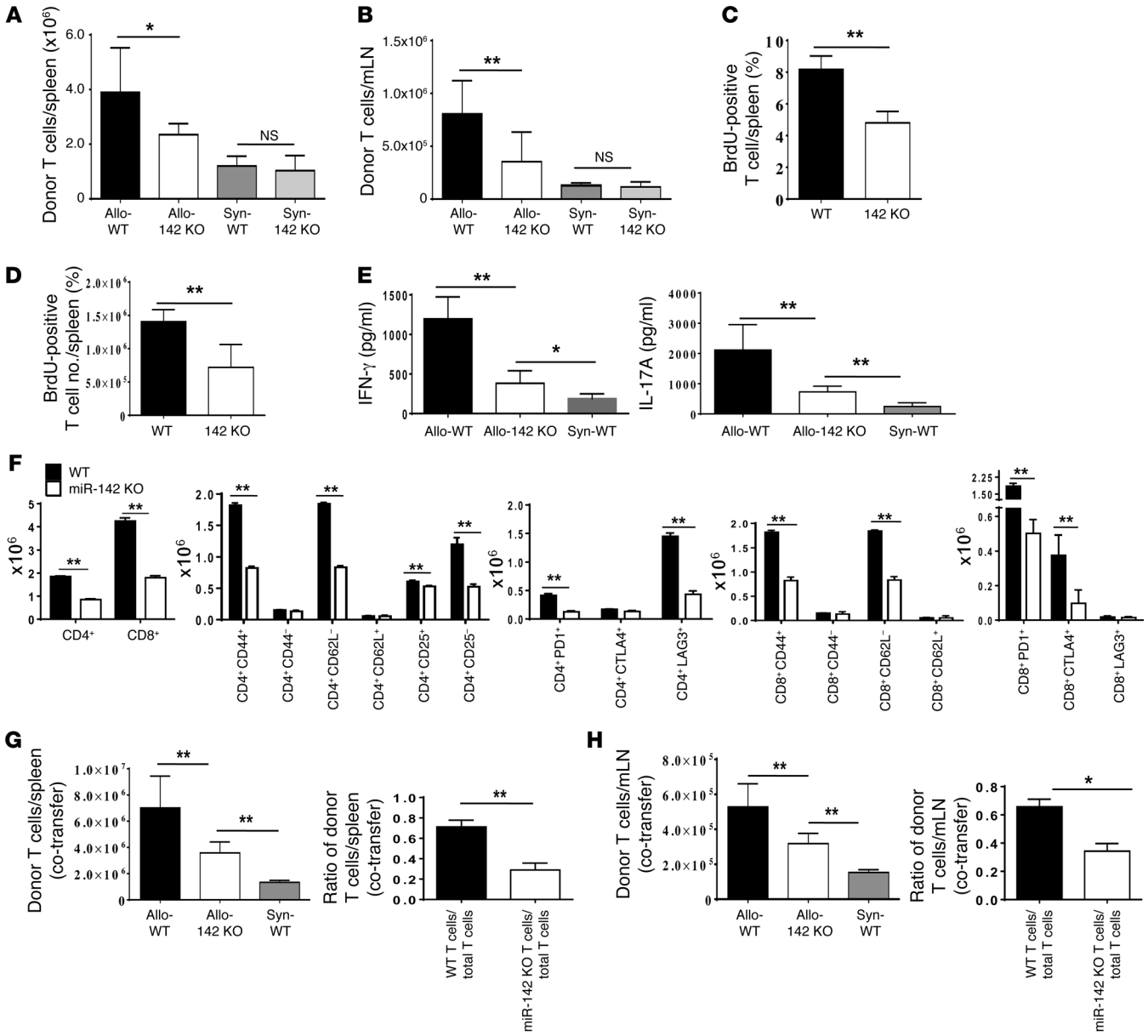

Figure 3. miR-142 KO T cells altered in cytokine expression and proliferative responses in vivo. (**A** and **B**) T cell proliferation in vivo. After 7 days in B6 into BALB/c BMT model, absolute donor T cell numbers for spleen (**A**) and mLN (**B**) were calculated from each individual animal. Data were combined from 2 independent experiments (n = 6–10). (**C** and **D**) BrdU incorporation in vivo. Similarly to what was shown in **A**, splenocytes were stained with Abs against $H2^b$, CD3, and BrdU. Percentages (**C**) and absolute T cell numbers (**D**) positive for BrdU were calculated by gating for $H2^{b+}$, $CD3^+$, and $BrdU^+$. Data were combined from 2 independent experiments (n = 6–10). (**E**) Cytokine expression in vivo. Using sera collected from transplanted mice as in **A**, concentrations of IFN-γ and IL-17A were measured by ELISA. Data were combined from 3 independent experiments (n = 12–14). (**F**) Phenotype analyses of transferred donor T cells. Similarly to what was shown in **A**, splenocytes were analyzed with FACS (n = 4). (**G** and **H**) WT and miR-142 KO T cells cotransfer model. Using modified BMT model as shown in **A**, T cells from either WT mice (ly5.2/CD45.1) or miR-142 KO mice (ly5.1/CD45.2) were cotransferred into the BALB/c recipients. After 7 days, donor T cells in spleen (**G**) and mLN (**H**) were analyzed using FACS staining. The ratios of 2 populations were analyzed based on total donor T cells obtained. Data were combined from 2 independent experiments (n = 6–10). Data were mean ± SEM. $^*P < 0.05$; $^{**}P < 0.01$, by unpaired t test for (**A**–**F**) and paired t test for (**G** and **H**).

cells showed significantly improved survival (58% versus 0%; $P < 0.01$) (Figure 4A) and reduced clinical severity of GVHD ($P < 0.01$) (Figure 4B). Detailed histopathological analyses of GVHD target organs confirmed allogeneic animals that received T cells from miR-142–deficient donors had significantly reduced histopathological GVHD in the gastrointestinal tract ($P < 0.01$), liver ($P < 0.05$) (day 14 and 21) (Figure 4, C and D), and skin ($P < 0.01$) on day +21 (Figure 4D) after BMT.

We next tested, in a different MHC mismatched mouse BMT model, B6 ($H2^b$) into B6D2F1 (F1, $H2^{bxd}$), using B6 into B6 as a syngeneic control. Recipient F1 mice were conditioned and transplanted from either WT B6 or miR-142 KO mice as described in Methods. Similarly, less severe GVHD (Figure 4E) and improved survival were observed in the allogeneic animals that received T cells from miR-142 KO donors compared with the recipients of allogeneic WT T cells (58.3% versus 16.6%,

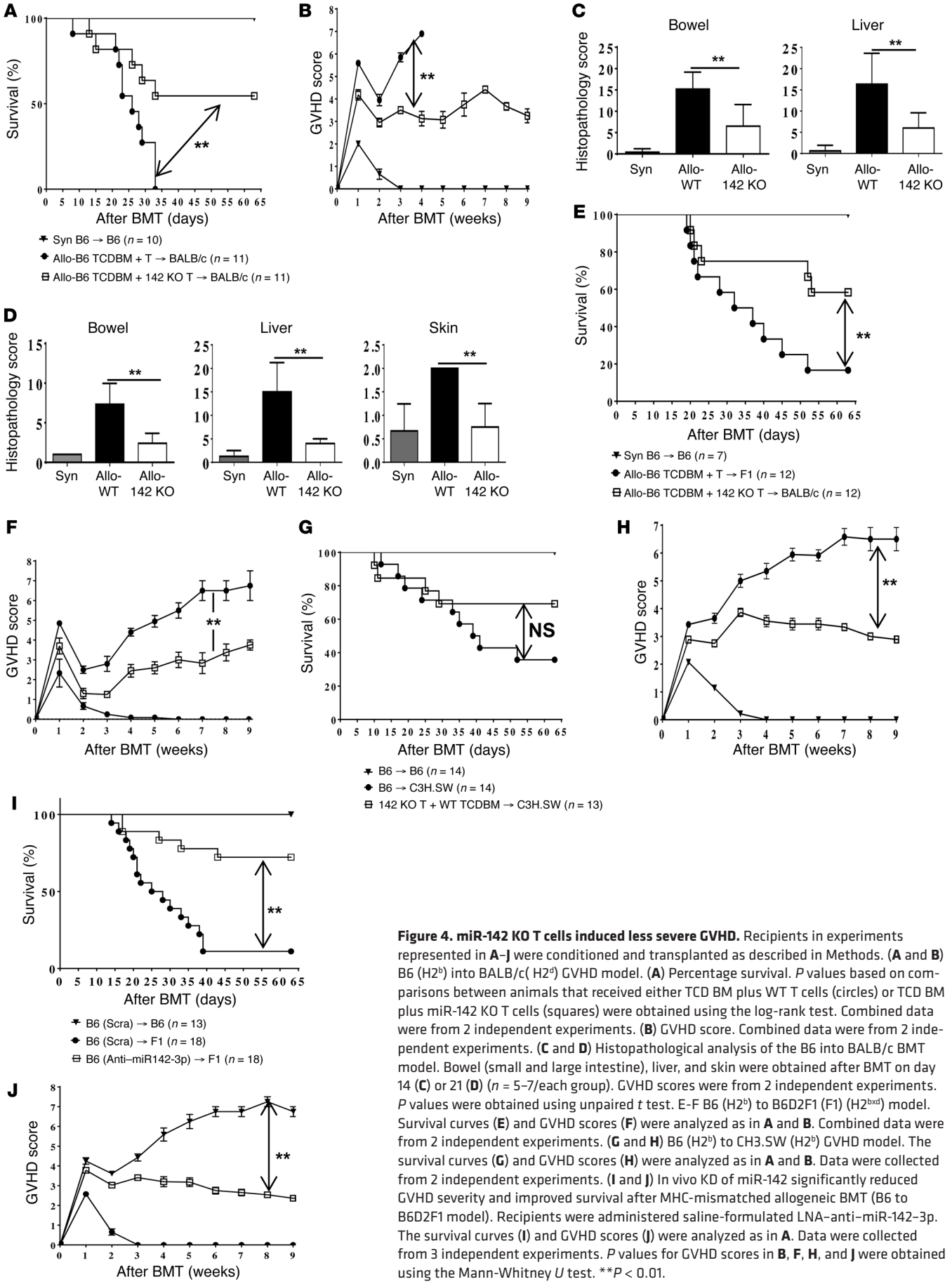

Figure 4. miR-142 KO T cells induced less severe GVHD. Recipients in experiments represented in **A**–**J** were conditioned and transplanted as described in Methods. (**A** and **B**) B6 ($H2^b$) into BALB/c($H2^d$) GVHD model. (**A**) Percentage survival. *P* values based on comparisons between animals that received either TCD BM plus WT T cells (circles) or TCD BM plus miR-142 KO T cells (squares) were obtained using the log-rank test. Combined data were from 2 independent experiments. (**B**) GVHD score. Combined data were from 2 independent experiments. (**C** and **D**) Histopathological analysis of the B6 into BALB/c BMT model. Bowel (small and large intestine), liver, and skin were obtained after BMT on day 14 (**C**) or 21 (**D**) (*n* = 5–7/each group). GVHD scores were from 2 independent experiments. *P* values were obtained using unpaired *t* test. E-F B6 ($H2^b$) to B6D2F1 (F1) ($H2^{bxd}$) model. Survival curves (**E**) and GVHD scores (**F**) were analyzed as in **A** and **B**. Combined data were from 2 independent experiments. (**G** and **H**) B6 ($H2^b$) to CH3.SW ($H2^b$) GVHD model. The survival curves (**G**) and GVHD scores (**H**) were analyzed as in **A** and **B**. Data were collected from 2 independent experiments. (**I** and **J**) In vivo KD of miR-142 significantly reduced GVHD severity and improved survival after MHC-mismatched allogeneic BMT (B6 to B6D2F1 model). Recipients were administered saline-formulated LNA–anti–miR-142–3p. The survival curves (**I**) and GVHD scores (**J**) were analyzed as in **A**. Data were collected from 3 independent experiments. *P* values for GVHD scores in **B**, **F**, **H**, and **J** were obtained using the Mann-Whitney *U* test. $^{**}P < 0.01$.

$P < 0.01$). Clinical GVHD was also less severe in animals that received miR-142 KO allogeneic T cells ($P < 0.01$) (Figure 4F).

Next, to determine whether miR-142 deficiency had functional relevance in in vivo model systems wherein T cell stimulation was less robust than observed in MHC disparate allostimulation, we utilized an MHC-matched, but multiple minor antigen–disparate model of BMT. To this end, we utilized a well-established model, B6 ($H2^b$) into CH3.SW ($H2^b$), in which pathological responses are directed at multiple minor H antigenic differences between donors and recipients (20). Lethally irradiated C3H.SW mice received transplants of WT B6 TCD BM (5×10^6) and purified splenic T cells from either WT B6 or miR-142–deficient mice. As shown in Figure 4G, animals that received allogeneic miR-142–deficient T cells showed a trend, but not statistically significant improved survival, after BMT compared with WT controls (69.2% versus 35.7%, $P = 0.075$). However, the clinical scores were significantly lower than in animals that received WT allogeneic T cells (Figure 4H, $P < 0.01$).

In vivo KD of miR-142 with antagomir mitigates GVHD. To further confirm the role of miR-142 and to determine whether targeting miR-142 might have therapeutic value, we tested the effect of in vivo blockade of miR-142 with its antagomir using the B6 into F1 MHC mismatched BMT model. The B6 and F1 recipients were lethally irradiated and transplanted with B6 TCD BM and splenic T cells. Allogeneic F1 animals were treated with miR-142 antagomir or scrambled controls at a dose of 10 mg/kg on days 1, 3, and 7. We observed that cells harvested following treatment at the above doses showed completely blocked expression of miR-142 (9). As shown in Figure 4, I and J, 90% of the allogeneic F1 animals that received the control antagomir died with signs of severe GVHD (Figure 4I). In contrast, 75% of the allogeneic recipients that were treated with the antagomir survived with minimal signs of GVHD (Figure 4J), suggesting that targeting miR-142 in vivo reduces GVHD.

miR-142 affects T cell cycling following stimulation. We next sought to determine the cellular mechanisms underlying the reduced proliferative capacity of miR-142–deficient T cells. We explored the cellular mechanisms by kinetically examining the cell cycling using flow cytometric analyses of DNA content with propidium iodide (PI) staining. Purified T cells from either WT or miR-142–deficient mice were stimulated with anti-CD3 and anti-CD28 Abs and analyzed for $subG_1$ G_1, S, G_2/M, and >4C phases of the cell cycle (Supplemental Figure 4, A–C). Following stimulation, the percentage of miR-142–deficient T cells in the $subG_1$ phase, (a stage that includes the late stage of apoptosis) was similar to the percentage of WT T cells in the $subG_1$ phase on days 0 to 2; however, on day 3, the percentage of miR-142–deficient T cells in the $subG_1$ phase was higher than the percentage of WT T cells. On day 4, the percentage of miR-142–deficient T cells in the $subG_1$ phase decreased, whereas the percentages of WT T cells in the $subG_1$ phase continued to increase (Supplemental Figure 4, B and C). These observations were consistent with observations using annexin V staining (Figure 1, E and F) in which miR-142 KO T cells showed reduced apoptosis only after longer stimulation (day 4). In contrast, the percentages of miR-142–deficient T cells in the G_1 phase, the growth phase, were significantly lower than those of WT T cells ($P < 0.01$; Supplemental Figure 4C). Moreover, the percentages of miR-142–deficient T cells in phase >4C were lower during days 1–3 than those of WT T cells, but they were similar on day 4 (Supplemental Figure 4C). These data demonstrated that miR-142 deficiency in T cells resulted in reduced cell proliferation both early and also on later days, thus accounting for reduced T cell expansion despite reduction in apoptosis at later time points.

Molecular profiling of miR-142–deficient T cells. To understand the molecular mechanisms underlying the cell-cycle alterations, we purified naive splenic T cells from either miR-142–deficient mice or WT littermates in triplicate and performed DNA microarray analyses. The upregulated genes in miR-142–deficient T cells were analyzed using gene function concept (conceptgen.ncibi.org) based on multiple databases, including Gene Ontology (GO; http://geneontology.org/) and Medical Subject Headings (MeSH; https://www.nlm.nih.gov/mesh/) (Supplemental Table 1). The highlighted functional concepts were ranked by *P* and *Q* (false discovery rate [FDR]) values from GO and MeSH analyses, which demonstrated that the cell-cycle–related functional concepts were the most highly ranked (Figure 5, A and B). We next extracted 168 genes that were upregulated and fell into the cell-cycle functional concept by GO analysis (Supplemental Table 1). These 168 genes were first filtered by selecting the probe sets with fold changes of 2 or greater to prevent large fold changes based on 2 small numbers. Twenty-nine genes were removed at this step.

Expression data for the remaining 139 genes were applied to gene set enrichment analysis (GSEA), and 35 genes yielded enrichment scores greater than 0.5 (Figure 5C, Supplemental Table 2, and Supplemental Figure 5). Next, we further analyzed the top 35 genes (according to enrichment score > 0.5 listed in Supplemental Table 2) with GeneMANIA (http://genemania.org/) for gene set function network prediction. As shown in Supplemental Figure 6, the functional network of DNA replication was most highly ranked. Seven genes that function in the DNA replication functional network were significantly highlighted by the analysis (Figure 5D). Interestingly, multiple E2F family members, a group of genes that includes a family of transcription factors (TFs) in higher eukaryotes that are involved in cell-cycle regulation and DNA synthesis in mammalian cells (21), were among these 139 genes. Notably, the atypical E2F family members, *E2f7* and *E2f8*, were ranked among the top 5 and 7, respectively, with enrichment scores of 0.871125 and 0.8333576, while the typical E2F family members (*E2f1* to *E2f6*) were ranked lower (Supplemental Table 2).

Validation of microarray results. We focused on the atypical E2F family members, E2F7 and E2F8, because (a) they were among the most differentially expressed genes; (b) they can form homo- or heterodimers with each other to repress the cell cycle (21) and induce S phase arrest (22–29); and (c) they are predicted as direct targets of miR-142 by multiple bioinformatics programs (data not shown). To confirm these observations, we searched for expression values (log_2) of the top 7 upregulated genes (*Anxa1*, *Evi5*, *Anln*, *Ccne2*, *E2f7*, *Esco2*, and *E2f8*) in miR-142 KO and WT T cells in original triplicate microarray files and obtained consistent results with our bioinformatics analyses (Supplemental Figure 7). We next confirmed the microarray data by finding that the mRNA expression levels of both *E2f7* and *E2f8* were significantly higher in miR-142–deficient T cells compared with WT T cells by qPCR (Figure 6A and Supplemental Figure 8A); the expression levels of these genes were

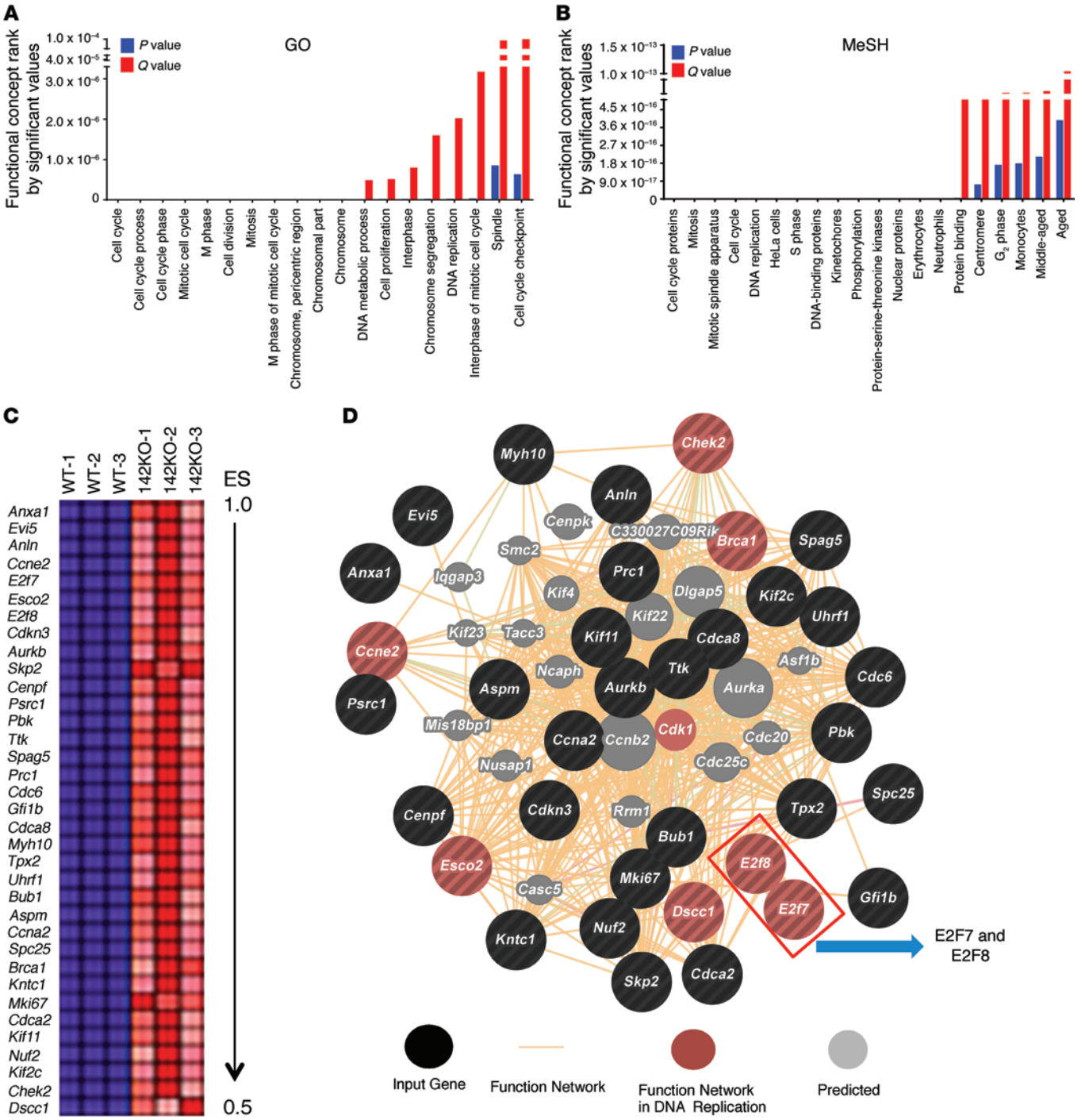

Figure 5. Upregulated genes in miR-142 T cells were markedly highlighted in the cell-cycle functional network. (**A** and **B**) Upregulated genes in miR-142 KO T cells identified in Affymetrix microarray were analyzed for gene function concept based on multiple databases, including GO (**A**) and the MeSH database (**B**). The analyzed data were ranked by *P* values (blue bars) and *Q* values (FDR, red bar). Data were obtained from 3 biological triplicates. (**C**) The gene set that is involved in the cell-cycle function concept was analyzed for enrichment by GSEA. The top 35 genes received 0.5–1 enrichment scores. The enrichment score ranking list is shown in Supplemental Table 2. Data were obtained from 3 biological triplicates. (**D**) The top 35 enriched genes were further analyzed for function network by GeneMANIA. Atypical E2F proteins (E2F7 and E2F8) were highlighted in the function network of DNA replication. Data were obtained from 3 biological triplicates.

also higher at the protein level as shown by Western blot (Figure 6B). Immunocytochemistry (ICC) showed E2F7- or E2F8-positive staining only in a portion of T cells from either WT or miR-142 KO mice (Figure 6C), likely because that atypical E2F protein expression is dependent on the stage of cell cycling (S or G_2 phase), as reported previously (21). Importantly, miR-142 KO T cells showed significantly stronger staining for E2F7 and E2F8 (Figure 6C). We also confirmed upregulated expression of *Anxa1*, (30), which was

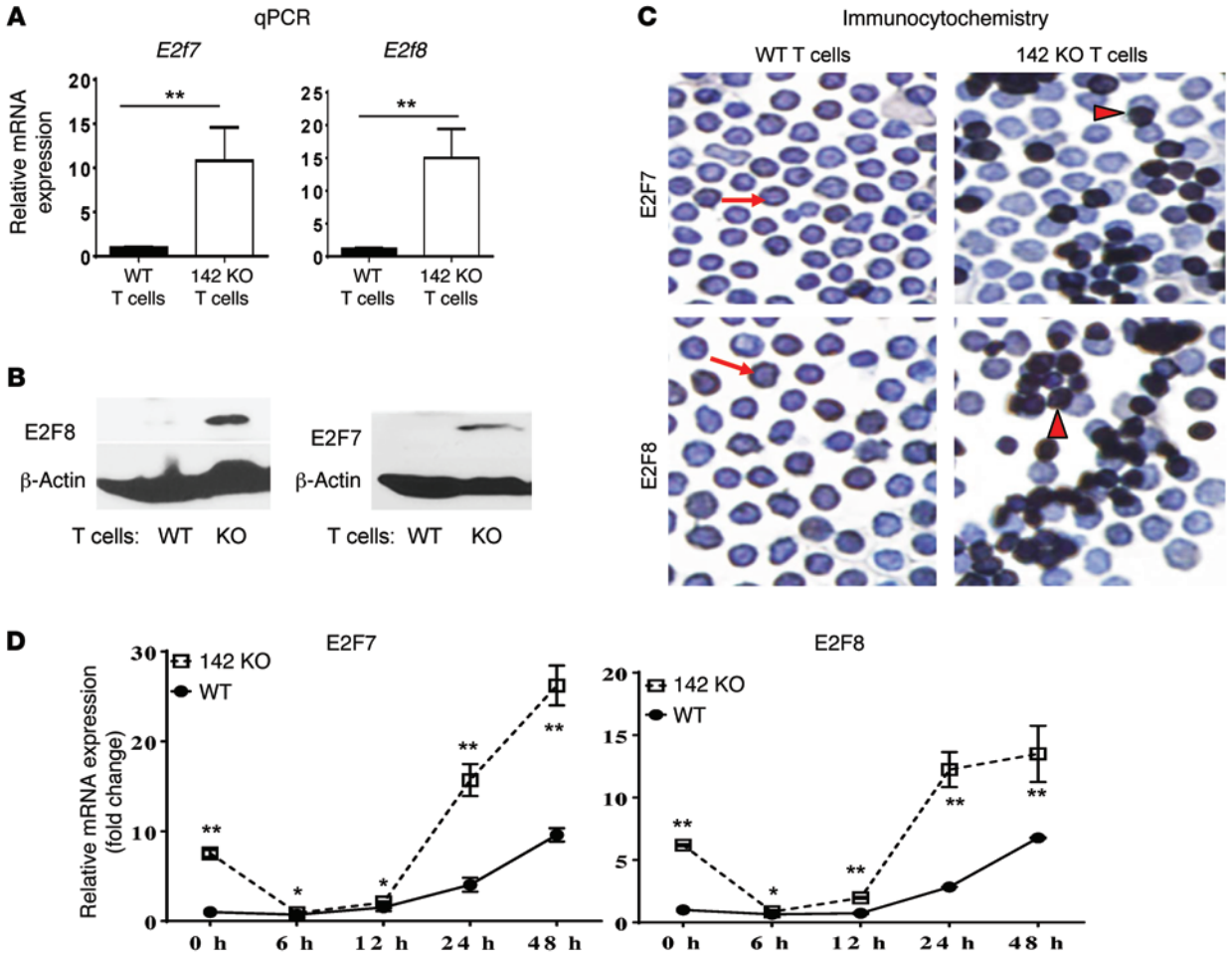

Figure 6. Atypical E2F proteins were significantly upregulated in miR-142 KO T cells. (**A**) Confirming upregulated *E2f7* and *E2f8* in miR-142 KO T cells using qPCR. Combined results (mean ± SEM) were from 3 independent experiments as shown in Supplemental Figure 10A. *P* values were obtained using the unpaired *t* test. (**B**) Western blotting demonstrated that E2F7 and E2F8 were upregulated in miR-142 KO T cells. Data are representative of 3 independent experiments. (**C**) Confirming upregulated E2F7 and E2F8 in miR-142 KO T cells using ICC. Purified T cells from either miR-142 KO or WT mice were spread onto polylysine-precoated slides by cytocentrifugation and processed for ICC with specific Abs against E2F7 and E2F8. Dark brown staining in cytoplasm was observed, as indicated by arrows. Much stronger (darker brown) staining was observed in miR-142 KO T cells, as indicated by arrowheads. Data are representative of 3 similar experiments. Original magnification, ×400. (**D**) Significantly increased expression of E2F7 and E2F8 in response to anti-CD3 and anti-CD28 Ab stimulation. Dynamic observation of expression of E2F7 and E2F8 in response to in vitro stimulation with anti-CD3 and anti-CD28 Abs was conducted for 0–48 hours. Data represent combination of 3 independent experiments (mean ± SEM). *P* values were obtained using multiple *t* test. $^{*}P < 0.05$; $^{**}P < 0.01$.

ranked as the most upregulated gene in the cell-cycle pathway in miR-142 KO T cells (Supplemental Figure 8B) and in both $CD4^+$ and $CD8^+$ KO T cell subsets (Supplemental Figure 8B).

We further examined the kinetic expression of E2F family in T cells in response to anti-CD3 and anti-CD28 stimulation. Expression levels of *E2f1*, *E2f2*, *E2f3*, *E2f4*, *E2f5*, and *E2f6* were similarly modulated in miR-142–deficient and WT T cells (Supplemental Figure 9); however, the *E2f7* and *E2f8* genes were differentially expressed, characterized by high expression in naive cells, but still significantly greater upregulation in miR-142–deficient T cells (Figure 6D). These data collectively suggest that upregulation of E2F7 and E2F8 may have a functional impact on T cells (22, 23).

miR-142 regulates T cell cycling in an E2F7/E2F8-dependent manner. To investigate the roles of E2F7 and E2F8 in T cell cycling, we first tested the functional consequences of E2F7 and E2F8 overexpression on WT T cells. WT T cells transduced with lentiviral particles expressing E2F7 or E2F8 were treated with anti-CD3 and anti-CD28 Abs for different periods of time, and their cell cycling was analyzed as above. Overexpression of E2F7 and E2F8 in WT T cells significantly induced S and G_2/M phase arrests in T cells (Figure 7A and Supplemental Figure 10, A and B). Of note, we did not observe significant differences in T cell phenotypes after infection with either control or E2F7/E2F8 overexpression lentiviral particles (Supplemental Figure 10C). We also observed a reduction in the proliferative capacity of T cells expressing E2F7 and E2F8, as demonstrated by ^{3}H-TdR incorporation assays (Figure 7B), similar to the observations made using miR-142 KO T cells (Figure 1E), suggesting tha E2F7 and E2F8 play an important role in normal WT T cell cycling.

We next examined whether the increased expression of E2F7 and E2F8 in miR-142 KO T cells was relevant to the cell-cycling defects observed in the absence of miR-142. To this end, we utilized the CRISPRi system (sgRNA-dCas9 complex, where sgRNA indicates single-guide RNA) for targeted silencing of transcription (31,

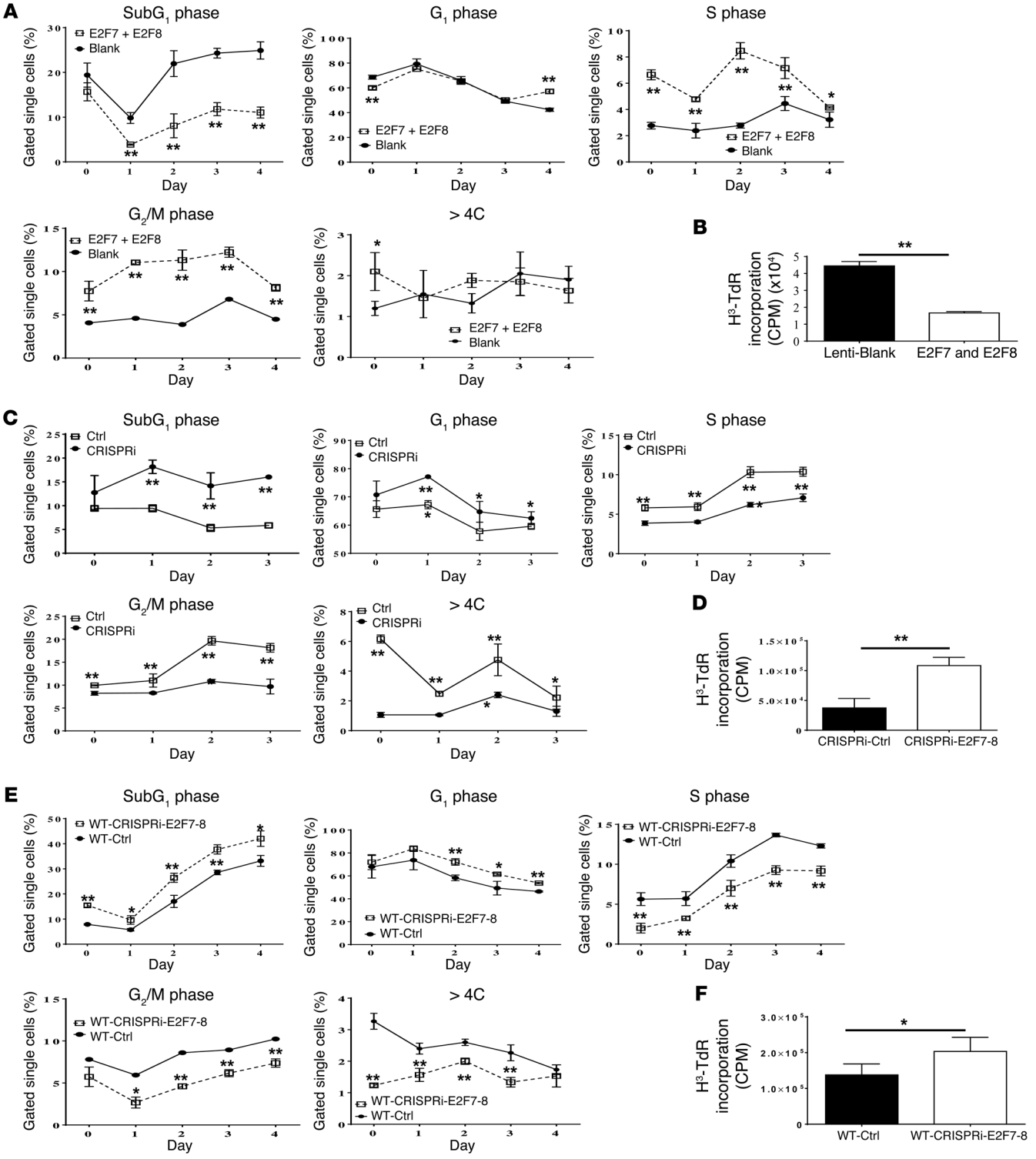

Figure 7. miR-142 regulates T cell cycling in E2F7/E2F8-dependent manner. (**A**) Impact of overexpression of atypical E2F proteins on cell cycle in WT T cells. WT T cells were infected with E2F7/E2F8 lentiviral particles, treated with anti-CD3 and anti-CD28 Abs, and analyzed for cell cycle. Combined data were from 3 independent experiments. (**B**) Overexpression of E2F7/E2F8 significantly inhibited T cell proliferation, as demonstrated by ^{3}H-TdR incorporation. Data represent combination of 3 independent experiments. (**C**) Impact of E2F7/E2F8 silencing on cell cycle in miR-142 KO T cells. miR-142 KO T cells were targeted for E2F7/E2F8 silencing as described in Methods, then treated with anti-CD3 and anti-CD28 Abs for 0 to 3 days. Cell-cycle analyses were processed. Combined data were from 3 independent experiments. (**D**) KD of E2F7/E2F8 in miR-142 KO T cells significantly improved cell proliferation, as demonstrated by ^{3}H-TdR incorporation. Data represent combination of 3 independent experiments. (**E**) Essential role of E2F7/E2F8 in cell-cycle activities in WT T cells. WT T cells were targeted for E2F7/E2F8 silencing, treated with anti-CD3 and anti-CD28 Abs for 0 to 4 days, and processed for cell-cycle analyses as in **C**. Data were combined from 3 independent experiments. (**F**) KD of E2F7/E2F8 in WT T cells significantly enhanced cell proliferation as demonstrated by ^{3}H-TdR incorporation. Data represent combination of 3 independent experiments. Data are shown as mean ± SEM. $^*P < 0.05$; $^{**}P < 0.01$, Holm-Sidak method (**A**, **C**, and **E**); unpaired *t* test (**B**, **D**, and **F**).

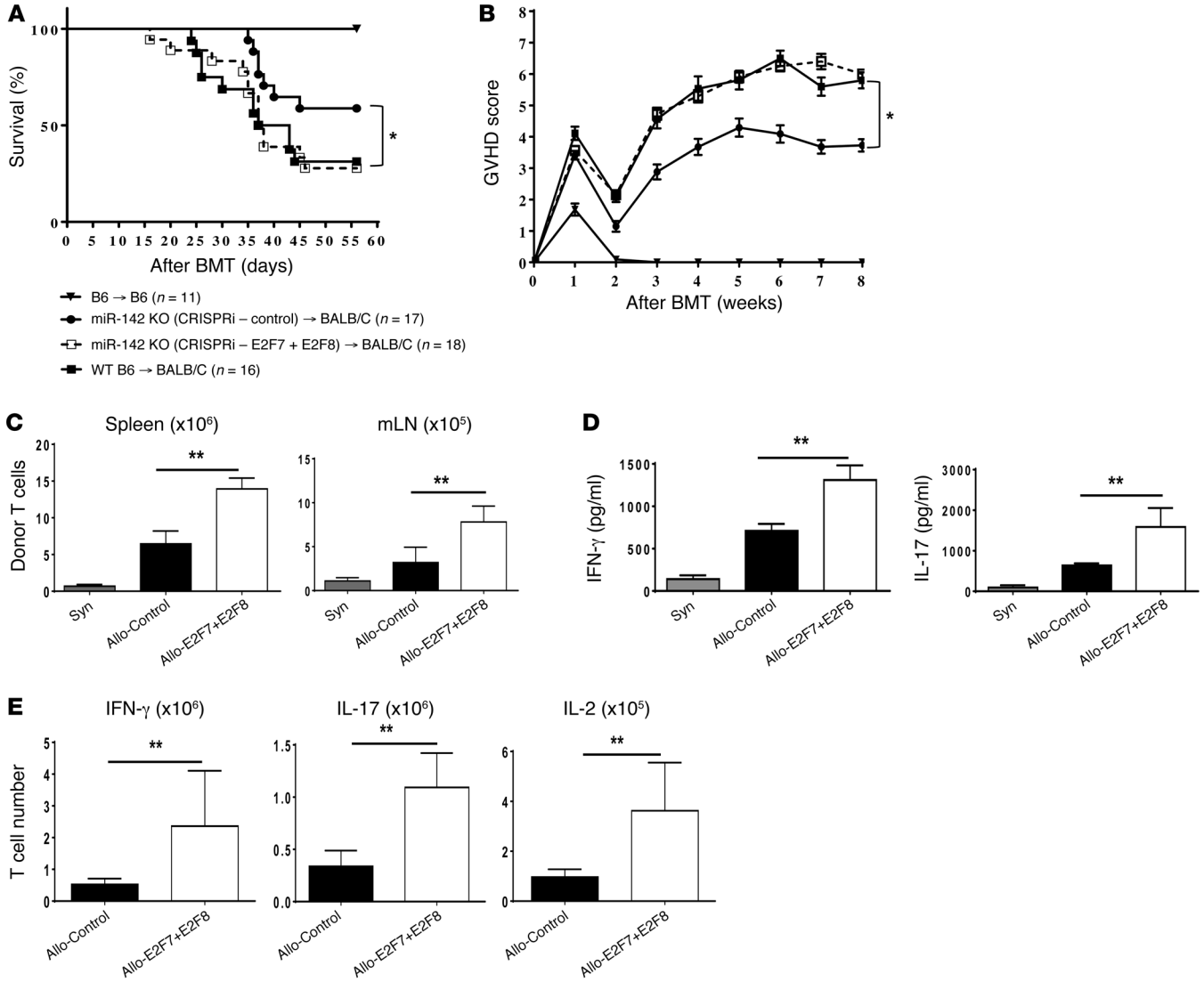

Figure 8. Upregulated expression of E2F7/E2F8 in miR-142 KO T cells contributes to reduced GVHD. (**A** and **B**) B6 to BALB/c GVHD model. Targeted silencing of E2F7/E2F8 in miR-142 KO T cells was processed as described in Methods. Recipients were conditioned and transplanted as in Figure 4A. Percentage survival (**A**) and GVHD score (**B**). Data were from 2 independent experiments. (**C**) Improved in vivo proliferation of miR-142 KO T cells after targeted silencing of atypical E2Fs. T cell expansion was examined on day 7 after BMT as in **A**. Absolute numbers of donor T cells in spleen and mLN were analyzed as described in Methods. Data were from 5 mice in each group (mean ± SEM). (**D**) Enhanced cytokine expression in vivo after targeted silencing of E2F7/E2F8 in miR-142 KO T cells. Concentrations of IFN-γ and IL-17A in sera from mice as in **C** were measured by ELISA (mean ± SEM). Data were combined from 5 mice in each group. (**E**) Increased absolute numbers of T cells expressing IFN-γ, IL-17A, and IL-2 in miR-142 KO T cells after targeted silencing of E2F7/E2F8. Splenic T cells from **C** were processed for intracellular staining for IFN-γ, IL-17A, and IL-2 as described in Methods. Combined results were from 5 mice for each group (mean ± SEM). $^*P < 0.05$; $^{**}P < 0.01$, log-rank test (**A**), Mann-Whitney U test (**B**), unpaired *t* test (**C**–**E**).

32) of the *E2f7* and *E2f8* in KO T cells. We cloned and concatenated 2 sgRNAs onto the same plasmids to form multiple sgRNA expression cassettes specific for either E2F7 or E2F8 and developed the lentiviral particles sg7AB and sg8AB (see detailed design procedures in Methods). The miR-142 KO T cells were infected with lentiviral particles that express either negative sg-control, sg7AB, or sg8AB from a murine polymerase III U6 promoter along with lentiviral particles that express dCas9 for 3 days. *E2f7* and *E2f8* expression levels were then measured by qPCR, and the cell cycle was analyzed by flow cytometry. We observed that transfection with lentiviral particles for dCas9 and either sg7AB or sg8AB successfully inhibited *E2f7* and *E2f8* mRNA expression, respectively, in miR-142 KO T cells. However, lentiviral transfection itself did not significantly affect T cell phenotype (Supplemental Figure 11, A and B). KD of E2F7 and E2F8 influenced the T cell cycle by reducing S and G_2/M phase arrests (Figure 7C and Supplemental Figure 11C) and increasing T cell proliferative capacity (Figure 7D). We also observed an increased frequency of late apoptotic cells (subG_1 phase) and 4C phase cells after CRISPRi KD of atypical E2Fs (Supplemental Figure 11C and Figure 7C), demonstrating the antiapoptotic and cell-cycle repressor roles for atypical E2F proteins (22–29).

We next determined whether the KD of atypical E2Fs will influence cell cycling in WT T cells. The WT T cells were transduced with CRISPRi lentiviral particles either for silencing

E2F7/8 or as negative control as above and processed for cell-cycle analyses as shown in Figure 7C. KD of E2F7 and E2F8 in WT T cells decreased cell populations in S, G_2/M, and >4C phases, but increased cell population in subG_1 and G_1 phases (Figure 7E), and enhanced T cell proliferation (Figure 7F). However, no significant differences were observed in T cell phenotype after infection with either control or CRISPRi–E2F7/E2F8 lentiviral particles (Supplemental Figure 12C).These data demonstrate that "physiological" levels of E2F7 and E2F8 expression are necessary for normal cell-cycle activities in T cells (20, 21, 22), while their overexpression in the absence of miR-142 is important for the cell-cycling defects shown by the KO T cells.

Upregulated expression of atypical E2F7 and E2F8 in miR-142 KO T cells contributes to reduced GVHD. To determine the contribution of atypical E2F-mediated cell-cycling alterations to the in vivo proliferative defects and associated GvHD reduction of miR-142 KO T cells, we targeted for E2F7/E2F8 silencing by the CRISPRi system in the B6 miR-142 KO T cells. They were then utilized in an allogeneic B6 ($H2^b$) → BALB/c ($H2^d$) model of GVHD. Allogeneic and syngeneic recipient mice were conditioned as described in Methods. Briefly, allogeneic BALB/c recipients were transplanted with 1×10^6 purified miR-142 KO T cells that had either been infected with lentiviral particles carrying double-guide RNAs targeting atypical E2Fs or CRISPRi-control along with dCas9 lentiviral particles for 3 days or control WT cells. Syngeneic B6 recipients were transplanted with 5×10^6 TCD WT B6 BM cells along with 1×10^6 purified WT B6 T cells, which were infected with lentiviral particles carrying CRISPRi-control along with dCas9 lentiviral particles for 3 days. The recipients were monitored for survival and clinical severity of GVHD. All of the syngeneic animals survived. In contrast, as shown in Figure 8, A and B, allogeneic animals that received miR-142 KO T cells transduced with atypical E2Fs silencing lentiviral particles showed greater clinical GVHD severity and higher mortality than the allogeneic animals that received miR-142 KO T cells transduced with CRISPRi-control lentiviral particles (58.8% versus 27.8% $P < 0.01$), but GVHD severity and mortality that were similar to those of allogeneic animals that received WT T cells (27.8% vs. 26%, P = NS).

Furthermore, the allogeneic miR-142 KO donor T cells targeted for silencing of atypical E2Fs also showed significantly increased expansion in recipient spleens and mesenteric LNs on day +7 after BMT when compared with allogeneic animals that received miR-142 KO donor T cells infected with CRISPRi-control (Figure 8C). The increased expansion of donor miR-142 KO T cells targeted for silencing of atypical E2Fs in vivo was also associated with increased production of IFN-γ and IL-17A, as determined by ELISA (Figure 8D) and by intracellular staining for IFN-γ, IL-17A, and IL-2 (Figure 8E). These data collectively demonstrate that upregulated expression of atypical E2Fs in miR-142 KO T cells contributes to reduced GVHD, in vivo T cell proliferation, and cytokine expression.

Discussion

miRs can activate or repress an innate or adaptive immune response, depending on their ability to modulate specific genes in specific cellular subsets (3–6, 33). Interestingly, while a few miRs have been reported as playing a role in immunity and naive T cell development and in homeostasis, the functional roles for specific miRs in regulating mature T cell response upon activation and modulating T cell–mediated disease have not been robustly demonstrated. In this study, we generated miR-142 KO mice that were viable, fertile, and showed normal T cell development. However, when the miR-142 KO T cells were activated ex vivo or in vivo following adoptive transfer, they demonstrated marked alterations in functions and ability to cause T cell–mediated immune-pathologies such as GVHD in multiple well-characterized mouse models of BMT. An important observation was that along with reduced T cell proliferation in miR-142 KO T cells, cytokine expression was also reduced. We utilized 3 well-characterized mouse models of BMT. Compared with T cells from WT littermates, miR-142 KO T cells displayed significantly reduced recovery and expansion as determined by BrdU incorporation studies in vivo ($P < 0.01$). These results were consistent with in vitro ^{3}H-TdR incorporation studies. Furthermore, cotransfer experiments demonstrated that the reduced proliferation and expansion of miR-142–deficient T cells were attributable to intrinsic features, but not environmental influences.

Our study demonstrated marked defects in T cell cycling by the miR-142–KO animals as the potential cellular mechanism for reduction in in vitro and in vivo T cell expansion. Compared with T cells from WT littermates, miR-142 KO T cells showed significant S and G_2/M phase arrest and reduced proliferative capacity ($P < 0.01$). Molecular profiling studies showed that the loss of miR-142 in T cells induced significant upregulation of genes that control the cell cycle ($P < 0.001$). Through systematic analyses of these genes, we specifically observed that atypical E2F family proteins, E2F7 and E2F8, play pivotal roles in regulating cell cycling in WT T cells and are also critical for the defects observed in the KO T cells. Thus, these data demonstrate what we believe to be a novel and hitherto unknown role for atypical E2Fs in T cell proliferation and reveal deeper insights into the molecular mechanisms of atypical E2F proteins in these processes; we also show that the atypical E2F proteins are regulated by miR-142.

We also observed reduced apoptosis in miR-142–deficient T cells on day 4 and afterwards upon stimulation with anti-CD3 and anti-CD28 Abs or allogeneic splenocytes (Figure 1, E and F). E2F7 and E2F8 cooperatively provide an important constraint against excessive E2F1 activation, which has long been known to be a potent stimulator of apoptosis (22, 23, 26, 27). Upregulated E2F7 and E2F8 expression may contribute to the reduced apoptosis in miR-142–deficient T cells. We also observed differential apoptosis between miR-142 KO T cells and T cells that overexpressed E2F7 or E2F8 by showing that more marked apoptosis (subG_1 phase) occurred in E2F7- or E2F8-overexpressing T cells than in miR-142 KO T cells. This observation suggested that the proper compensation and cooperative function among genes involved in relative functional networks occurred in miR-142 KO T cells; however, in E2F7- or E2F8-overexpressing T cells, this gene network was not functional, yet it could still compensate for the effects produced by E2F7 or E2F8 overexpression.

Consistent with our previous KD studies, we observed increased IL-6 production in naive miR-142–deficient T cells and after stimulation. Similar results were also observed in miR-142–deficient DCs activated with LPS, confirming previous observations that miR-142 targets IL-6 (9). However, the exact

mechanisms for the reduced expression of other cytokines, IFN-γ, IL-17A, and IL-2, in miR-142 KO T cells are unknown and whether these are related to defects in cell cycling will be pursued in future studies. The reduction of these cytokine, IFN-γ and/or IL-17, levels may have also contributed to the reduced GVHD in vivo (2). Furthermore, our data do not directly rule any potential contribution from other antiinflammatory molecules, such as AnxA1, a phospholipase A2 inhibitor with antiinflammatory activity, that may be targets of miR-142 (30, 34). Nonetheless, our data with CRISPRi KD of atypical E2F suggest that targeting of these 2 miR-142 targets is sufficient for reduction in GVHD.

The expression of miR-142 is limited to hematopoietic cells under homeostatic conditions (9, 10, 35). However, it is possible that its temporal expression may be observed in other tissues, especially under stress; this remains largely unexplored. Like many miRs, miR-142 likely can target multiple genes and the genetic programs may vary depending on the cell type and context. The complete KO animals generated by us did not show any defects in numbers of HSCs when compared with WT animals (data not shown). Recent data have suggested a role for miR-142 in other hematopoietic-derived cell functions, such as regulatory T cell function (19), myeloid cell differentiation (9, 12, 13), and megakaryopoiesis (14). Furthermore, in association with other aberrations, it has also been incriminated in the development of hematopoietic malignancies (16, 17) and even nonhematopoietic cells and malignancies (18, 36).

Our data demonstrate that expression of miR-142 has clear functional implications for T cell functional biology. Furthermore, we achieved in vivo KD of miR-142 using LNA–anti–miR-142 administrated before and after allogeneic BMT and showed that short-term use improved the severity of GVHD and reduced mortality after allogeneic HSCT, similar to the effects observed by miR-142 KO T cells. In addition to T cells, the in vivo KD approach targets miR-142 in all hematopoietic cells, such as B cells, antigen-presenting cells (APCs), and BM cells. Thus, the clinical impact on GVHD with this approach, while complementary to the miR-142 KO T cells, is likely a net result of the impact on other hematopoietic cells as well. Nonetheless, these observations suggest that a short-term miR-142 KD with antagomirs may be a potential therapeutic strategy for T cell–mediated and other immune-mediated diseases such as GVHD.

Methods

Gene targeting and development of KO mice. The murine genomic clone, RP23-449P23, containing the *Mir142* gene was obtained from the BACPAC Resources Center (http://bacpac.chori.org). A replacement vector that was designed to replace the miR-142 hairpin precursor (bp 100001–1000064) and upstream 1,000 bp (bp 99040–100001) as well as downstream 2,640 bp (bp 100064–102705) with a PGK-neomycin–resistance cassette was constructed. Details are in the Supplemental Methods. Briefly, the targeting vector was delivered into the JM8.F6 (C57BL/6N) stem cell by microinjection. Targeted heterozygotes were monitored by genotyping using TaqMan real-time qPCR (37). The ES-derived from B6 mouse substrains (JM8.F6 [C57BL/6N] stem cell) and carrying targeting vector was injected into albino B6 mice to produce black-on-white chimeras. ES cell–mouse chimeras with high coat color contribution from the ES cells (90%) were selected for germline transmission. Pups produced from sperm derived from the B6 host embryo had black coats and those from the albino B6 host embryo were white. Tail biopsies from the pups were screened for the presence of the targeted gene. The absence of the *Mir142* gene was further confirmed by TaqMan qPCR. The absence of miR-142 expression in *Mir142*$^{-/-}$ mice was confirmed in BM tissues and T cells isolated from spleen using specific probes against miR-142–3p, using Raw264.7 cells as positive control and NIH3T3 cells as negative control (11). The details of the oligos used and the 5′ and 3′ sequences are shown in the Supplemental Methods.

Mice. B6 ($H2^b$, CD45.2), C3H.sw ($H2^b$), BALB/c ($H2^d$), B6D2F1 ($H2^{b/d}$, CD45.2), and B6 Ly5.2 ($H2^b$, CD45.1) mice were purchased from The Jackson Laboratory and the National Cancer Institute. The age of mice used for experiments ranged between 8 and 12 weeks. Mice were housed in sterilized microisolator cages and received filtered water and normal chow.

DC isolation, BMT, and systemic analyses of GVHD. DC and cell isolation along with BMTs were performed as described before and are detailed in Supplemental Methods (38–40). Briefly, recipient BALB/c mice received an 800-cGy TBI on day –1 (split dose) as well as T cells (1×10^6, isolated from either WT B6 mice or miR-142–deficient mice) and TCD BM cells (5×10^6, from WT B6 mice). B6D2F1 mice received a 1100-cGy TBI on day –1 as well as T cells (2.5×10^6, isolated from either WT B6 mice or miR-142–deficient mice). Recipient C3H.SW mice received a 1050-cGy TBI on day –1 as well as T cells (1.5×10^6, isolated from either WT B6 mice or miR-142–deficient mice). For in vivo KD of miR-142–3p using LNA–anti–miR-142–3p, recipient B6D2F1 and B6 mice were administered saline-formulated LNA–anti–miR-142–3p or LNA mismatch control by the injection volume of 200 μl with an i.p. dose of 10 mg/kg, respectively, on days 1, 3, and 7 (9). For in vivo CRISPRi-targeted silencing of atypical E2Fs using the B6 into BALB/c GVHD model as described above, purified miR-142 KO T cells were infected with lentiviral particles carrying double-guide RNAs targeting E2F7 and E2F8 or CRISPRi-control for 3 days. The recipient BALB/c mice were transplanted as detailed in Supplemental Methods. Survival was monitored daily. The degree of clinical GVHD and histological grading were assessed by a standard scoring system as before; this is detailed in Supplemental Methods (40).

T cell transfer and proliferation experiments. Details are provided in Supplemental Methods. Briefly, to examine the proliferation capability of miR-142 KO T cells following allogeneic BMT, 1×10^6 purified WT or miR-142–deficient T cells were injected i.v. into the BALB/c recipients on day 0 after irradiation along with WT TCD BM cells (5×10^6), and the donor T cells in spleen and mLNs were analyzed 7 days later by staining for $H2^{b+}CD90.2^+$. To assess intrinsic deficiency of miR-142, KO and WT T cells were cotransferred i.v. into the BALB/c recipients on day 0. After 7 days, donor T cells in spleen and mLN were analyzed using FACS staining gated for $H2^{b+}CD90.2^+CD45.1^+$ for WT donor T cells and $H2^{b+}CD90.2^+CD45.2^+$ for miR-142–deficient donor T cells. For BrdU incorporation experiments, WT B6 T cells and miR-142 KO T cells were injected i.v. into the BALB/c recipients on day 0 after irradiation. After 7 days of BMT, mice were injected with 50 mg/kg BrdU (5 mg/ml in 0.9% saline, i.p.) 3 hours prior to tissue collection.

Cytospin slide preparation, ICC, and cell-cycle measurement. Details are provided in the Supplemental Methods. Briefly, we used the Histo-Mouse-MAX Kit (Life Technologies) and Abs against E2F7 and E2F8 for ICC. Nuclear DNA content and cell-cycle measurements of WT or miR-

Table 1. Primer sequences for sgRNA cloning

Name	Sequence	Purpose
E2F7 FA	5′-GGAGAACCACCTTGTTGGggggtgaagattctttgctttgac**GTTTTAGAGCTAGAAATAGCAAGTTAAAATAAGGC**-3′	Construct sgRNAs on U6 vectors
E2F7 FB	5′-GGAGAACCACCTTGTTgggaacgcatcctccttattctcaat**TCGTTTTAGAGCTAGAAATAGCAAGTTAAAATAAGGC**-3′	
E2F8 FA	5′-GGAGAACCACCTTGTTGGgcttctttcaatacacgaagtaCT**GTTTTAGAGCTAGAAATAGCAAGTTAAAATAAGGC**-3′	
E2F8 FB	5′-GGAGAACCACCTTGTTGGggagcgcacgagcccgggttccga**GTTTTAGAGCTAGAAATAGCAAGTTAAAATAAGGC**-3′	
E2F R	5′-CCTAGTACTCGAGAAAAAAAGCACCGACTCGGTGCCACTTTTTCAAGTTGATAACGGACTA**GCCTTATTTTAACTTGCTATTTCTAGCTCTAAAAC**-3′	
E2F F-control	5′-GGAGAACCACCTTGTTGG**GTTTTAGAGCTAGAAATAGCAAGTTAAAATAAGGC**-3′	
E2F F-double	5′-GCCGCGAGATCTGAGATCCGACGCGCCATC-3′	Construct tandem sgRNAs on the U6 vector
E2F R-double	5′-AATAACTAATGCATGGCGGTAATACGGT-3′	
pU6 F-seq	5′-GAGATCCAGTTTGGTTAGTACCGGG-3′	Sequencing primers for U6 vector
pU6 R-seq	5′-ATGCATGGCGGTAATACGGTTAT-3′	

Underlines indicate restriction sites, lower-case letters indicate the bp region, and bold indicates the complementary sequence.

142 KO T cells were processed and analyzed using the CycleTEST PLUS DNA Reagent Kit (BD Biosciences). The area parameter histogram was used to determine the percentage of cells in G_1, S, G_2/M, and >4C phases.

Affymetrix microarrays and analyses. The translational control RNA (tcRNA) was extracted from purified WT B6 T cells and miR-142 KO T cells with the RNeasy Mini Kit (QIAGEN). Details of the microarrays and the analyses are in the Supplemental Methods. Briefly, Affymetrix mouse genome 430 2.0 arrays (Affymetrix) were used. The stained arrays were scanned on an Agilent Gene Array Scanner (Affymetrix) with a 560-nm filter. Data were published and analyzed using the R statistical environment (http://cran.r-project.org/) provided by Bioconductor (http://www.bioconductor.org/) and were examined for quality control by showing the same distribution of the PM probes for each chip and no degradation. The expression values were then calculated for each gene using a robust multi-array average (41, 42). The gene set that was involved in the specific function concept was analyzed for enrichment by GSEA (http://www.broadinstitute.org/gsea/index.jsp), and the top enriched genes were further analyzed for function network by GeneMANIA (http://www.genemania.org/). All original microarray data were deposited in the NCBI's Gene Expression Omnibus (GEO GSE57543).

CRISPRi system, sgRNA design, cloning, lentiviral packaging, and T cell infection. CRISPRi system, sgRNA design, cloning, lentiviral packaging, and T cell infection were performed as before (19–24) and are detailed in Supplemental Methods. Briefly, the CRISPRi system, derived from the Streptococcus pyogenes CRISPR pathway, requiring only the coexpression of a catalytically inactive Cas9 protein and an sgRNA, was chosen to KD E2F7 and E2F8 (31, 32). pHR-SFFV-dCas9-BFP-KRAB (Addgene, 46911) was utilized to express dCas9, which lacks endonucleolytic activity because of carrying 2 point mutations in both its RuvC-like (D10A) and HNH nuclease (H840A) domains (43). For sgRNA design, first, we selected exon 2 or exon 1 in E2F7 or E2F8 genome loci, which contain the PAM sites for dCas9 binding as the targets (see details in Supplemental Methods), then designed oligos to obtain chimeric sgRNA, which contain the sequences encoding dCas9 handle and transcription terminator derived from S. pyogenes. To achieve the crucial interaction between dCas9 and the dCas9 handle hairpin for target binding, the prediction of secondary structure folding of the dCas9 handle hairpin was processed for each sgRNA construct using the online Quikfold algorithm (http://mfold.rna.albany.edu/?q=DINAMelt/Quickfold).

Expression plasmids were cloned by inserting PCR products into the lentiviral U6-based expression vector (Addgene, 44248) digested by BstXI and XhoI. To obtain multiplexed targeting sgRNA plasmids, we inserted compatible restriction enzyme sites (BglII and BamHI) to flank individual sgRNA expression cassettes as BioBrick parts (44) to concatenate multiple sgRNA expression cassettes into a single expression vector. The target sequences of the 73 sgRNAs are shown below. The PAMs are in bold; the target sequences (19–24 nucleotides) are underlined and italicized and were used as the bp regions of the sgRNA. The sequences are as follows: *E2f7* exon 2: aaaatatatttgtcgaccgatcaaggatgaccccaaagacaccgatgaagaacgagccgatcga**CCT***gtcaaagcaaagaatcttcaccccc*agacagaaaccccattactccagtaaagccggtcgacaggcagccgcaggtggagccctggacacccacagccaacctgaagatgctcatcagcgccgccagcccagacataagagaccgggagaagaaaaaggagctgttcaga**CCC***attgagaataaggaggatgcgttcg*tgaactccctgcag; *E2f8* exon 1: 5′-agtgcttgcgccgggcgggacgcgggctactgctggggactgtacctgggaccgggagcgcagcgtacggtgcgctttggcatcgcggtgatttcggcacctagggaatccttccctcgc**CCC***agtacttcgtgtattgaaagaagcc*tgaaaaaggggtcaagatcccaaagccctttgtaaatgcccggtcgtgcgcttagagcgcagaggctgaattggagggttgttctcaggccacttcacaagtccttccttctgagcctgtgcacgtgtgtgtcaggcgagaaacttcagcatctccccgatgcaggctcggtgcgtgct**CCA***tcggaacccgggctcgtgcgctccg*tccgcagcccggatcagtgcacaggatagtaaa. See Table 1 for the sgRNA sequence for the E2F7/8 and controls.

Concentrated lentiviral particles carrying double-guide RNAs targeting E2F7 and E2F8, Cas9, or negative control constructs were prepared by Vector Core of Biomedical Research Core Facilities at the University of Michigan. miR-142 KO or WT T cells were infected with lentiviral particles carrying double-guide RNAs targeting E2F7 and E2F8 or negative control along with Cas9 lentiviral particles for 3 days with complete medium supplemented with Polybrene (Sigma-Aldrich) at a final concentration of 5 μg/ml. Infection efficiency was controlled under microscopy by fluorescence for BFP or mCherry infused in lentiviral constructs for dCas9 or sgRNA.

Lentiviral infection and PCR studies. Lentiviral infection and PCR studies were performed as detailed in Supplemental Methods. The primer data for all of the E2F family members are shown in Supplemental Methods.

Mixed lymphocyte cultures, CFSE, intracellular and annexin V FACS staining, and ELISA. Mixed lymphocyte cultures, carboxyfluorescein succinimidyl ester (CFSE), intracellular and annexin V FACS stain-

ing, and ELISA were performed as described before (11, 15, 38, 39, 40) and as detailed in Supplemental Methods.

Immunoblot analyses. Cell lysates were prepared from WT and miR-142 KO T cells and CD3/28 T cells. A 50-μg quantity of each protein extract was boiled in sample buffer, separated by SDS-PAGE, and transferred onto a PVDF membrane (GE Healthcare). The membrane was incubated for 30 minutes with 5% nonfat dry milk and then incubated overnight at 4°C with the following Abs: anti-E2F7 rabbit polyclonal Ab (1:1,000 in 5% nonfat milk; ab56022, Abcam), anti-E2F8 rabbit polyclonal Ab (1:1,000 in 5% nonfat milk; ab109569, Abcam), anti-AxnA1 rabbit polyclonal Ab (1:1,000 in 5% nonfat milk; catalog 3299 Cell Signaling), and anti-actin mouse mAb (1:1,000; Abcam). After washing with TBS-T, the blot was incubated with an HRP secondary Ab. The signals were visualized by enhanced chemiluminescence (Thermo Scientific).

Statistics. Data were analyzed using Prism GraphPad (version 5 or 6). The relevant statistics were clarified by a biostatistician. Briefly, comparisons between 2 groups were calculated using *t* test, while comparisons between 2 groups at multiple time points were calculated utilizing the Holm-Sidak method. The log-rank (Mantel-Cox) test was utilized to analyze all survival data. The Mann-Whitney *U* test was used for the statistical analysis of clinical scores (38, 39, 45–47). All of the gene expression and relative quantification data were analyzed on the log (base 2) scale. Comparisons of the gene expression values across the sample classes were performed using the paired 2-sample, 2-tailed Student's *t* test. Affymetrix microarray data were further analyzed for function concept by GO and MeSH databases. Gene sets for specific gene concepts were ranked by *P* value and/or *Q* value. Gene enrichment was analyzed with GSEA, and genes in the function network were determined by the GeneMANIA database. $P < 0.05$ was considered statistically significant.

Study approval. All animal studies were reviewed and approved of by the University Committee on Use and Care of Animals of the University of Michigan, based on University Laboratory Animal Medicine guidelines.

Acknowledgments

This work was supported by NIH grants CA-0173878 and CA-143379 (National Cancer Institute) and HL-090775 (National Heart, Lung, and Blood Institute) (to P. Reddy).

Address correspondence to: Pavan Reddy, 3312 CCGC, 1500 E. Medical Center Drive, University of Michigan Cancer Center, Ann Arbor, Michigan 48109, USA. Phone: 734.647.5954; E-mail: reddypr@umich.edu.

1. Ferrara JL, Levine JE, Reddy P, Holler E. Graft-versus-host disease. *Lancet*. 2009;373(9674):1550–1561.
2. Paczesny S, Hanauer D, Sun Y, Reddy P. New perspectives on the biology of acute GVHD. *Bone Marrow Transplant*. 2010;45(1):1–11.
3. Banerjee A, Schambach F, DeJong CS, Hammond SM, Reiner SL. Micro-RNA-155 inhibits IFN-γ signaling in CD4+ T cells. *Eur J Immunol*. 2010;40(1):225–231.
4. Haasch D, et al. T cell activation induces a noncoding RNA transcript sensitive to inhibition by immunosuppressant drugs and encoded by the proto-oncogene, BIC. *Cell Immunol*. 2002;217(1–2):78–86.
5. Rodriguez A, et al. Requirement of bic/microRNA-155 for normal immune function. *Science*. 2007;316(5824):608–611.
6. Thai TH, et al. Regulation of the germinal center response by microRNA-155. *Science*. 2007;316(5824):604–608.
7. Cobb BS, et al. T cell lineage choice and differentiation in the absence of the RNase III enzyme Dicer. *J Exp Med*. 2005;201(9):1367–1373.
8. Muljo SA, Ansel KM, Kanellopoulou C, Livingston DM, Rao A, Rajewsky K. Aberrant T cell differentiation in the absence of Dicer. *J Exp Med*. 2005;202(2):261–269.
9. Sun Y, et al. Targeting of microRNA-142-3p in dendritic cells regulates endotoxin-induced mortality. *Blood*. 2011;117(23):6172–6183.
10. Wu H, et al. miRNA profiling of naïve, effector and memory CD8 T cells. *PLoS One*. 2007;2(10):e1020.
11. Sun Y, et al. PU.1-dependent transcriptional regulation of miR-142 contributes to its hematopoietic cell-specific expression and modulation of IL-6. *J Immunol*. 2013;190(8):4005–4013.
12. Mildner A, et al. Mononuclear phagocyte miRNome analysis identifies miR-142 as critical regulator of murine dendritic cell homeostasis. *Blood*. 2013;121(6):1016–1027.
13. Sonda N, et al. miR-142-3p prevents macrophage differentiation during cancer-induced myelopoiesis. *Immunity*. 2013;38(6):1236–1249.
14. Chapnik E, et al. miR-142 orchestrates a network of actin cytoskeleton regulators during megakaryopoiesis. *Elife*. 2014;3:e01964.
15. Sun Y, et al. Allogeneic T cell responses are regulated by a specific miRNA-mRNA network. *J Clin Invest*. 2013;123(11):4739–4754.
16. Gauwerky CE, Huebner K, Isobe M, Nowell PC, Croce CM. Activation of MYC in a masked t(8;17) translocation results in an aggressive B-cell leukemia. *Proc Natl Acad Sci U S A*. 1989;86(22):8867–8871.
17. Robbiani DF, et al. AID produces DNA double-strand breaks in non-Ig genes and mature B cell lymphomas with reciprocal chromosome translocations. *Mol Cell*. 2009;36(4):631–641.
18. Chiou GY, et al. Epigenetic regulation of the miR142-3p/interleukin-6 circuit in glioblastoma. *Mol Cell*. 2013;52(5):693–706.
19. Huang B, et al. miR-142-3p restricts cAMP production in CD4+CD25− T-cells and CD4+CD25+ TREG cells by targeting AC9 mRNA. *EMBO Rep*. 2009;10(2):180–185.
20. Duffner U, et al. Role of CXCR3-induced donor T cell migration in acute GVHD. *Exp Hematol*. 2003;31(10):897–902.
21. Chen HZ, Tsai SY, Leone G. Emerging roles of E2Fs in cancer: an exit from cell cycle control. *Nat Rev Cancer*. 2009;9(11):785–797.
22. Li J, et al. Synergistic function of E2F7 and E2F8 is essential for cell survival and embryonic development. *Dev Cell*. 2008;14(1):62–75.
23. Moon NS, Dyson N. E2F7 and E2F8 keep the E2F family in balance. *Dev Cell*. 2008;14(1):1–3.
24. Westendorp B, Mokry M, Groot Koerkamp MJ, Holstege FC, Cuppen E, de Bruin A. E2F7 represses a network of oscillating cell cycle genes to control S-phase progression. *Nucleic Acids Res*. 2012;40(8):3511–3523.
25. Christensen J, et al. Characterization of E2F8, a novel E2F-like cell-cycle regulated repressor of E2F-activated transcription. *Nucleic Acids Res*. 2005;33(17):5458–5470.
26. Ouseph MM, et al. Atypical E2F repressors and activators coordinate placental development. *Dev Cell*. 2012;22(4):849–862.
27. Chen HZ, et al. Canonical and atypical E2Fs regulate the mammalian endocycle. *Nat Cell Biol*. 2012;14(11):1192–1202.
28. Lammens T, Li J, Leone G, De Veylder L. Atypical E2Fs: new players in the E2F transcription factor family. *Trends Cell Biol*. 2009;19(3):111–118.
29. Lilly MA, Duronio RJ. New insights into cell cycle control from the Drosophila endocycle. *Oncogene*. 2005;24(17):2765–2775.
30. Wallner BP, et al. Cloning and expression of human lipocortin, a phospholipase A2 inhibitor with potential anti-inflammatory activity. *Nature*. 1986;320(6057):77–81.
31. Larson MH, Gilbert LA, Wang X, Lim WA, Weissman JS, Qi LS. CRISPR interference (CRISPRi) for sequence-specific control of gene expression. *Nat Protoc*. 2013;8(11):2180–2196.
32. Chen B, et al. Dynamic imaging of genomic loci in living human cells by an optimized CRISPR/Cas system. *Cell*. 2013;155(7):1479–1491.
33. Xiao C, Rajewsky K. MicroRNA control in the immune system: basic principles. *Cell*. 2009;136(1):26–36.
34. Yang YH, et al. Deficiency of annexin A1 in CD4+ T cells exacerbates T cell-dependent inflammation. *J Immunol*. 2013;190(3):997–1007.
35. Chen CZ, Li L, Lodish HF, Bartel DP. MicroRNAs modulate hematopoietic lineage differentiation. *Science*. 2004;303(5654):83–86.
36. Sharma S, Liu J, Wei J, Yuan H, Zhang T, Bishopric NH. Repression of miR-142 by p300 and MAPK

is required for survival signalling via gp130 during adaptive hypertrophy. *EMBO Mol Med*. 2012;4(7):617–632.
37. Shitara H, Sato A, Hayashi J, Mizushima N, Yonekawa H, Taya C. Simple method of zygosity identification in transgenic mice by real-time quantitative PCR. *Transgenic Res*. 2004;13(2):191–194.
38. Reddy P, Maeda Y, Liu C, Krijanovski OI, Korngold R, Ferrara JL. A crucial role for antigen-presenting cells and alloantigen expression in graft-versus-leukemia responses. *Nat Med*. 2005;11(11):1244–1249.
39. Reddy P, et al. Histone deacetylase inhibition modulates indoleamine 2,3-dioxygenase-dependent DC functions and regulates experimental graft-versus-host disease in mice. *J Clin Invest*. 2008;118(7):2562–2573.
40. Hill GR, Crawford JM, Cooke KR, Brinson YS, Pan L, Ferrara JL. Total body irradiation and acute graft-versus-host disease: the role of gastrointestinal damage and inflammatory cytokines. *Blood*. 1997;90(8):3204–3213.
41. Irizarry RA, et al. Exploration, normalization, and summaries of high density oligonucleotide array probe level data. *Biostatistics*. 2003;4(2):249–264.
42. Mathew JP, et al. From bytes to bedside: data integration and computational biology for translational cancer research. *PLoS Comput Biol*. 2007;3(2):e12.
43. Qi LS, et al. Repurposing CRISPR as an RNA-guided platform for sequence-specific control of gene expression. *Cell*. 2013;152(5):1173–1183.
44. Shetty RP, Endy D, Knight TF Jr. Engineering BioBrick vectors from BioBrick parts. *J Biol Eng*. 2008;2:5.
45. Hill GR, et al. Differential roles of IL-1 and TNF-α on graft-versus-host disease and graft versus leukemia. *J Clin Invest*. 1999;104(4):459–467.
46. Jennrich RI. A note on the behavior of the log rank permutation test under unequal censoring. *Biometrika*. 1983;70(1):133–137.
47. Wu J. A new one-sample log-rank test. *J Biomet Biostat*. 2014;5:210.